Research Article

Pengfei Li, Minxian Shi, Zongyi Deng, Pengkun Han, Tingli Yang, Rui Hu, Chuang Dong, Rui Wang, and Jie Ding*

Achieving excellent oxidation resistance and mechanical properties of TiB_2–B_4C/carbon aerogel composites by quick-gelation and mechanical mixing

https://doi.org/10.1515/ntrev-2022-0489
received June 24, 2022; accepted September 14, 2022

Abstract: Thermal protection system (TPS) is of great significance to launch hypersonic flight and landing process of hypersonic vehicles, which can effectively shield the hypersonic vehicle from severe aerodynamic heating encountered. Phenolic aerogels play an important role in TPS due to their characteristics of low density, high porosity, and low thermal conductivity. However, phenolic aerogel is easy to be oxidized at elevated temperatures under oxidizing environments, which severely limits its large-scale application as thermal insulation materials in TPS. In this study, a novel TiB_2–B_4C/carbon (TB/C) aerogel composite was synthesized by introducing TiB_2 and B_4C particles into phenolic aerogels through quick-gelation and mechanical mixing. The developed aerogel composites were characterized by scanning electron microscopy, Fourier transform infrared, thermal analysis, *etc.*, to evaluate their microstructure, oxidation resistance, and mechanical properties. Experimental evidence showed that TiB_2 and B_4C particles reacted with the oxygen-containing molecules to form TiO_2–B_2O_3 layer, which effectively improved oxidation resistance and mechanical properties of phenolic aerogel composites.

Keywords: particle-reinforced composites, thermal properties, phenolic aerogel composites

*** Corresponding author: Jie Ding,** School of Materials Science and Engineering, Wuhan University of Technology, Wuhan, 430070, China, e-mail: jied@whut.edu.cn, tel: +86 15623626180.
Pengfei Li, Minxian Shi, Zongyi Deng, Pengkun Han, Tingli Yang, Rui Hu, Chuang Dong, Rui Wang: School of Materials Science and Engineering, Wuhan University of Technology, Wuhan, 430070, China

1 Introduction

Phenolic aerogels were widely used in hypersonic vehicles, civil structural edifices, and industrial architectures [1–3]. Incorporation of inorganic particles into a phenolic aerogel matrix can significantly improve mechanical, oxidation resistance, and fire retardancy of the organic–inorganic aerogel composites. However, phenolic aerogels are usually prepared *via* a week-long base-catalyzed gelation process, and deionized water or anhydrous ethanol is chosen as the solvent [4,5]. It is difficult to achieve well-dispersed inorganic particles in phenolic aerogels because of inorganic particle sedimentation due to gravity and incompatibility with precursor solution [6].

At present, there are two ways to modify the surface of inorganic particles by chemical treatments to increase the affinity of the inorganic particle surface for precursor solution [7,8]. The first one is accomplished through adding modified nanoparticles into polymer aerogels. Pulci *et al.* achieved surface modification of ZrO_2 nanoparticles with several organic acids, demonstrating that the addition of nano-ZrO_2 produces an improvement of both thermal and mechanical performance compared with pristine material [9]. The second method is using silane coupling agents to modify particle surfaces, thus improving the compatibility between the particle surfaces and precursor solution. Liu *et al.* used trimethoxy silane to modify halloysite nanotubes (m-HNTs) and introduced m-HNTs into the phenolic aerogel [10]. The obtained aerogel composite exhibited low carbonization shrinkage (30.83%) and enhanced residue yield (73.24%) at 1,000°C protected in N_2 atmosphere.

Functional inorganic particles, such as B_4C, TiB_2, and ZrB_2 particles, are generally considered as excellent candidates for thermal oxidation applications [11,12]. Compared with traditional inorganic particles, such as TiO_2,

ZrO_2, SiO_2, and Halloysite nanotubes, functional inorganic particles can react with oxygen-containing molecules to form oxides and increase the residue yield of composite during the oxidation process [13,14]. For example, TiB_2 particles react with the oxygen-containing molecules to form B_2O_3 and TiO_2 [15]. Besides, molten B_2O_3 cover the oxidized surface and form protective layer, which can effectively inhibit the oxidation of phenolic aerogel in the interior [16,17]. However, these functional inorganic particles are chemically inert and cannot be chemically treated to increase the compatibility of the particle surface for the solvent. For this reason, it is extremely difficult to efficiently introduce functional inorganic particles into phenolic aerogel.

In this work, a quick-gelation approach to achieve better dispersibility of TiB_2 and B_4C particles in the phenolic aerogel is reported. The gelation of resorcinol with formaldehyde could be remarkably accelerated by acid catalysis because the addition of formaldehyde is an electrophilic aromatic substitution reaction [18–21]. In Table 1, this work is compared with other existing works. As can be seen from Table 1, this work has ultra-quick time of gelation. Thus, trifluoroacetic acid (CF_3COOH) is used as a catalyst to accelerate gelation, which avoids the severe sedimentation of TiB_2 and B_4C particles over time in precursor solution. The oxidation of TiB_2 and B_4C particles at elevated temperatures could form a protective layer, which can effectively improve oxidation resistance and mechanical performance of aerogel composites. The introduction of TiB_2 and B_4C particles into phenolic aerogels in this study only requires simple mechanical mixing without complex chemical treatment, which is suitable for large-scale production.

2 Experimental

2.1 Materials

Formaldehyde (37.0 wt% aqueous solution, AR) and resorcinol (AR) were purchased from Aladdin Industrial Inc. Deionized water was supplied in our laboratory. CF_3COOH was obtained from Macklin Biochemical Co., Ltd. TiB_2 and B_4C particles (purity > 98%) with particle size of 1–10 μm, used as fillers, were provided by Aladdin Industrial Inc. All chemicals were used as-received with no further purification.

2.2 Preparation of TB/C aerogel composites

Figure 1 shows schematic illustration of the preparation process of TB/C aerogel composites. In this work, resorcinol, formaldehyde, and deionized water were referred to as R, F, and W, respectively. The molar ratios of F:R and W:R were maintained at 3:1 and 1:2, respectively. The weight ratio of TiB_2:B_4C was 1:1. According to the method, the precursor solutions, containing R, F, and W, were mixed by a magnetic stirrer at 35°C, and the solid content of the precursor solutions was recorded as 1. Suspension was manufactured by dissolving precursor solutions (solid content is 1) and 0, 10, 30, 50, 70, and 90% of filler (mixture of TiB_2 and B_4C) under vigorous stirring for 30 min, and then decanted into glass molds. Second, the appropriate amount of CF_3COOH was dropped into glass molds. The volume ratio of suspension:CF_3COOH was 20:1. The glass molds were sealed and placed into tube holder at room temperature for gelation to form hydrogels. Typically, the gel time is about 20–40 s and the aging time is 2 h. The obtained hydrogels were directly dried in an oven at 50°C for 24 h, 70°C for 24 h, and 90°C for 24 h to obtain aerogel composites. Finally, the samples were carbonized at 1,000°C for 20 min in muffle furnace. The uncarbonized phenolic (Ph) aerogel monomers were expressed as TB/Ph-*x*-*y*, and the carbon aerogel monomers were denoted as TB/C-*x*-*y*, where *x* refers to the content of TiB_2 and B_4C in TB/Ph-*x*-*y*, and *y* indicates carbonization temperature.

2.3 Characterization

The morphological microstructure of the samples was characterized by scanning electron microscopy (SEM;

Table 1: Comparison of gelation time of phenolic aerogels

Catalyst	Solvent	Molar ratio of R:F	Ratio of solvent catalyst	*T* (°C)	Gelation time	Ref.
Na_2CO_3	H_2O	1:2	72.5[a]	85	>2 days	[16,17]
HCl	CH_3CN	1:2	21[b]	80	10 min	[16]
CF_3COOH	H_2O	1:3	20[b]	35	15–30 s	This work

R: Resorcinol; F: formaldehyde; a: the molar ratio of solvent: catalyst; b: the volume ratio of solvent:catalyst.

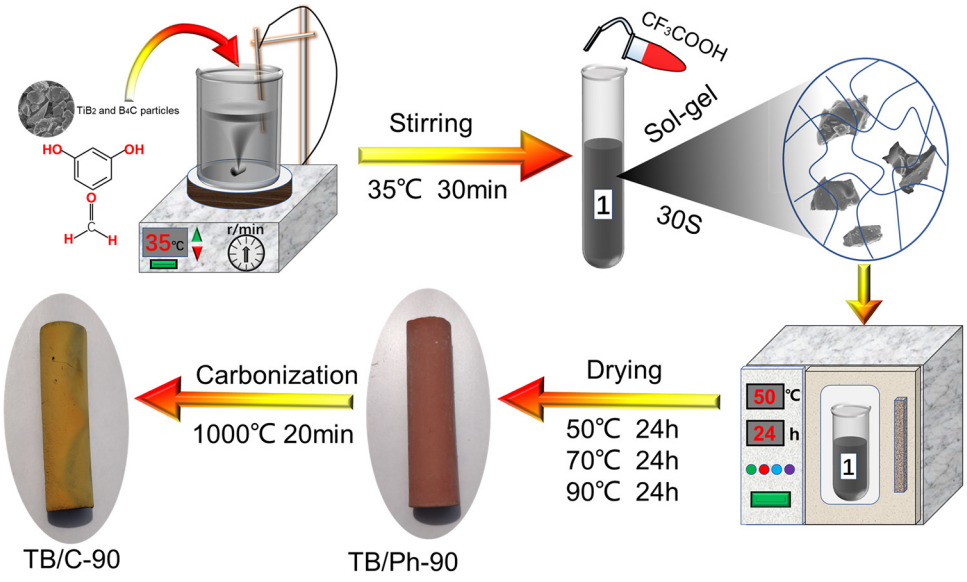

Figure 1: Schematic illustration for the preparation process of TB/C aerogel composites.

HitachiS-4800F) at an acceleration voltage of 10 kV. The groups of aerogel composites were characterized with Fourier Transform Infrared (FT-IR) spectra and recorded on a Nexus 670 FTIR spectrometer with KBr pellets in the wave number range of 4,000–500 cm^{-1}. Thermal stability test of the aerogel composites was performed by a NETZSCH STA449F3 thermal analyzer. Compressive strength of the cylindrical samples ($r \times h$: 10 mm × 20 mm) was measured by electronic universal testing machine with a testing speed of 1.0 mm min^{-1}. The XRD patterns of the TB/C aerogel composites were measured by an X-ray diffractometer, Bruker D8 Advance Discover with CuKα radiation (40 kV, 40 mA). The thermal residue of TB/C aerogel composites was also characterized by X-ray photoelectron spectroscopy (XPS). Drying and carbonization shrinkages were calculated by measuring the diameter of each cylindrical sample before and after drying and carbonization, respectively. Densities were determined through dividing weight by volume. Thermal conductivity was determined by the Hot Disk thermal protection system (TPS) 2500 thermal constant analyzer at 25°C.

3 Results and discussion

3.1 Microstructure of TB/C aerogel composites

The microstructures of the TB/C aerogel composites with different TiB_2 and B_4C contents are shown in Figure 2. SEM images show that TB/C aerogel composites are basically composed of well-connected microspheres, which are connected through clear neck and randomly gather together to obtain "grape string" appearance. For pure carbon aerogel without TiB_2 and B_4C added (Figure 2a), the diameter of carbon microspheres is about 1 μm and its surface is smooth. The morphology of samples begins to change as TiB_2 and B_4C particles are introduced, and in Figure 2b and c, the B_2O_3 layers start to appear and the TiO_2 grains are primitively generated. For TB/C-90 aerogel composites (Figure 2d2), the diameter of microspheres is about 620 nm.

The FTIR spectra of the TB/Ph aerogel composites with different TiB_2 and B_4C contents are shown in Figure 3a. The TB/Ph aerogel composites exhibited typical adsorptions of Ph–OH at 3,410 cm^{-1} (stretching), CH_2 stretching at 2,926 cm^{-1}, C═C vibration of aromatic rings at 1,617 and 1,476 cm^{-1}, Ph–O stretching vibrations of phenolic hydroxyl group at 1,220 cm^{-1}, and C–O stretching vibrations of methylene ether bridges (CH_2–O–CH_2) at 1,090 cm^{-1}. Bands at 1,015 cm^{-1} were ascribed to C–O stretching vibration of CH_2OH. The TB/Ph aerogel composites exhibited absorption peak of the hydrogen bonds (OH···O) at 3,224 cm^{-1} (Figure 3c) [22–24]. Presumably, hydrogen bonds (OH···O) are generated by the residual non-hydrolyzed hydroxymethyl groups (CH_2OH) and phenolic hydroxyl group (Ph-OH) [25]. As the content of TiB_2 and B_4C is increased, the intensity of the hydrogen bonds increases, indicating incorporation of more CH_2OH and Ph–OH in the form of hydrogen bonds.

Peaks at 1,617 cm^{-1} were assigned to the C═C vibration of aromatic rings, which were consistent in each

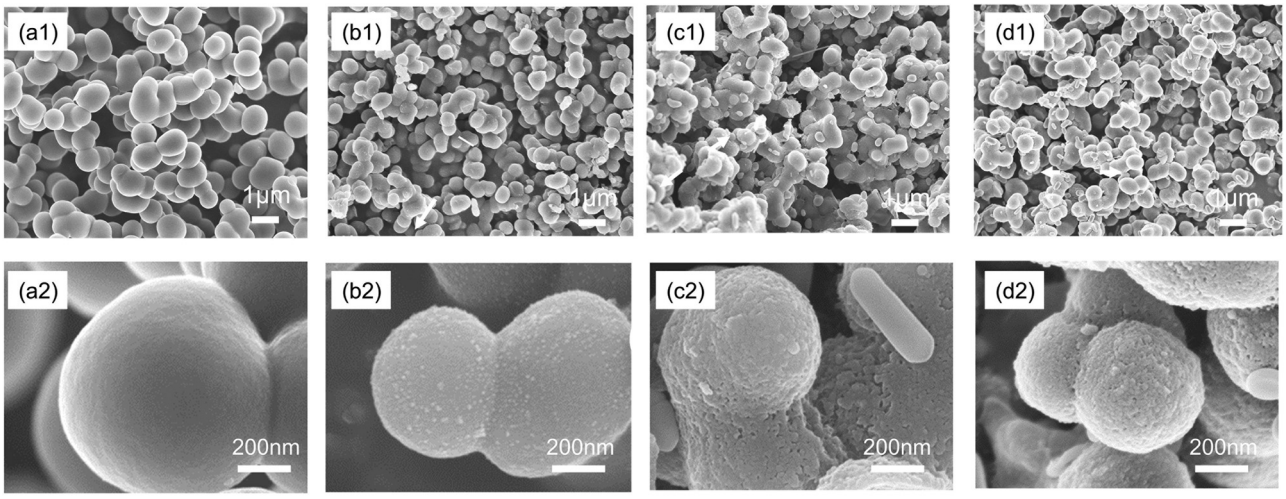

Figure 2: (a)–(d) SEM images of TB/C aerogel composites with different TiB_2 and B_4C contents: (a1), (a2) 0; (b1), (b2) 10%; (c1), (c2) 50%; and (d1), (d2) 90%.

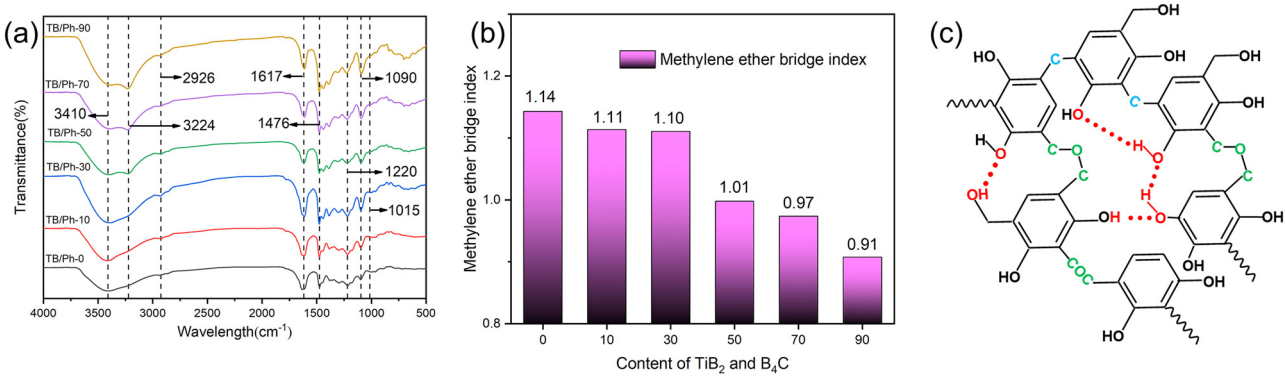

Figure 3: (a) FTIR spectra of TB/Ph aerogel composites, (b) methylene ether bridge index of TB/Ph aerogel composites, and (c) interactions of TB/Ph aerogel composites.

reaction system and unaffected by the content of TiB_2 and B_4C particles [26]. Thus, bands at 1,617 cm^{-1} could be used as a standard for analysis. The excessive formaldehyde (F/R = 3) allows the conjecture that most of the 2-, 4-, and 6-positions of the resorcinol aromatic rings react and form the corresponding hydroxymethyl derivatives. Thus, the molar ratio of methylene ether bridges (CH_2–O–CH_2) is much higher than that of methylene bridges (CH_2) in aerogel composites. Based on the absorption intensities (A_1 and A_0) of the methylene ether bridges and phenyl groups (1,090 and 1,617 cm^{-1}, respectively), we can calculate the methylene ether bridge index (I) of the TB/Ph aerogel composites by the following relationship: $I = A_1/A_0$. As shown in Figure 3b, it is apparent that the methylene ether bridge index decreases from 1.14 to 0.91 with the increased content of TiB_2 and B_4C, which was attributed to the added TiB_2 and B_4C particles hindering the motion of organic clusters and eventually partial CH_2OH and Ph-OH had not participated in the sol–gel reaction. This can result in different thermal stability and compressive strength of TB/Ph aerogel composites due to fewer methylene ether bridges [27–29]. All these are consistent with the FTIR spectra, TG, and comprehensive strength analysis.

3.2 Oxidation resistance and thermal stability of TB/Ph aerogel composites

3.2.1 TG-DTG analysis

As shown in Figure 4b and Table 2, the temperature of the maximum degradation rates (T_{max1}) for pure phenolic

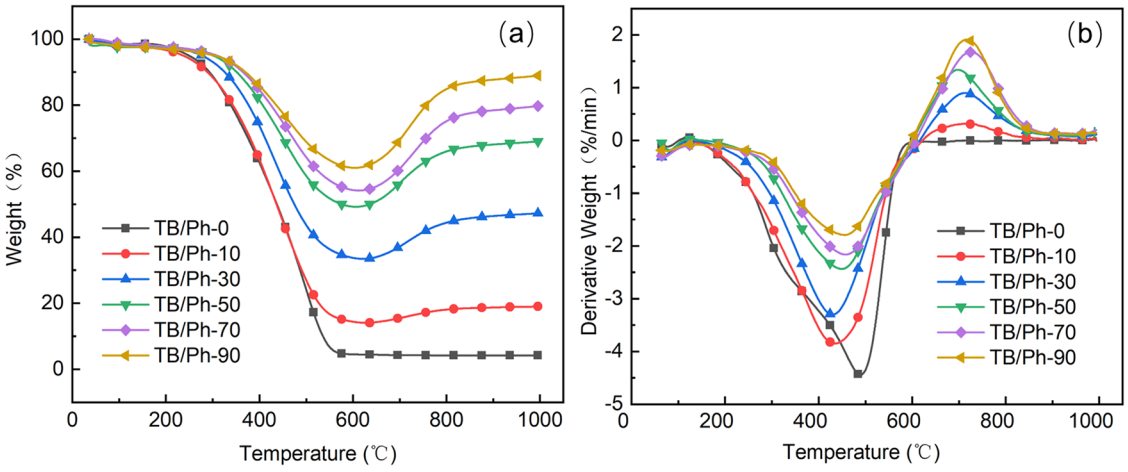

Figure 4: (a) TG curves of samples at a heating rate of 10°C min^{-1} from room temperature to 1,000°C under air atmosphere; (b) DTG curves of samples at a heating rate of 10°C min^{-1} from room temperature to 1,000°C under air atmosphere.

Table 2: Thermal decomposition characteristics of TB/Ph aerogel composites

Samples	T_{max1}/°C	T_{max2}/°C	Residue yield%		
			300°C	600°C	1,000°C
TB/C-0	494.4	/	88.75	5.8	5.68
TB/C-10	437.0	717.3	88.04	16.51	21.45
TB/C-30	429.7	712.6	92.55	35.37	49.25
TB/C-50	458.3	706.6	95.29	51.01	70.83
TB/C-70	455.8	724.7	95.10	54.02	79.83
TB/C-90	455.8	716.5	95.03	61.97	90.01

T_{max1}: temperature of the maximum degradation rate. T_{max2}: temperature of the maximum mass gain rate.

aerogel (494.4°C) are greater than that for TB/Ph aerogel composites. These results reveal that the thermal stability of aerogels is decreased clearly with the introduction of TiB_2 and B_4C particles by mechanical mixing. TiB_2 and B_4C particles will affect the condensation between hydroxymethyl derivatives of resorcinol and lead to a reduction in the number of methylene ether bridges (CH_2–O–CH_2). These are consistent with the FTIR spectra analysis. Moreover, with the increase in TiB_2 and B_4C particle content, T_{max1} increases slightly, as the formation of B_2O_3-protected structure will increase the T_{max1}. This should be attributed to oxidation of partial B_4C particles at temperatures below 500°C [30]. Interestingly, we discover that the residue yield of TB/Ph aerogel composites at high temperatures could be evidently increased by the presence of TiB_2 and B_4C particles. The residue yield of pure phenolic aerogel was 5.68%, while that of TB/Ph-90 hold was 90.01% at 1,000°C, indicating the outstanding oxidation resistance of TB/Ph aerogel composites.

As shown in Figure 4a and Table 2, the degradation processes of TB/Ph aerogel composites both can be divided into three stages [31]. Take the TB/Ph-90 for example, the first stage with little mass loss (<5%) is from room temperature to 300°C, and the mass loss of the samples is mainly due to the evaporation of the free water in the aerogels. When the temperature reaches 600°C, severe mass loss is observed in the TG curves. With the pyrolysis of phenolic aerogels, many kinds of pyrolysis volatiles including H_2O, CO, CO_2, H_2, CH_4, and other derivates are released out [32,33]. The oxygen-containing molecules, including CO, O_2, CO_2, and H_2O, take a large proportion in the number of volatiles, and provide a source of oxidizing atmosphere. In the step of 600–1,000°C, the residue yield of the TB/Ph aerogel composites increased continuously with the increased content of TiB_2 and B_4C particles, which means that some weight gain reactions between TiB_2 and B_4C particles and oxygen-containing molecules should have occurred. As listed in Table 2, the residue yield of TB/Ph-90 aerogel composites increased from 61.97 to 90.01%, when temperature was increased from 600 to 1,000°C. Some main gain reactions are given as follows:

$$2TiB_2(s) + 5O_2(g) = 2TiO_2(s) + 2B_2O_3(l,s), \quad (1)$$

$$TiB_2(s) + 5CO(g) = TiO_2(s) + B_2O_3(l,s) + 5C(s), \quad (2)$$

$$2TiB_2(s) + 5CO_2(g) = 2TiO_2(s) + 2B_2O_3(l,s) + 5C(s), \quad (3)$$

$$TiB_2(s) + 5H_2O(g) = TiO_2(s) + B_2O_3(l,s) + 5H_2(g), \quad (4)$$

$$B_4C(s) + 5O_2(g) = 2CO_2(g) + 2B_2O_3(l,s), \quad (5)$$

$$B_4C(s) + 6H_2O(g) = C(s) + 2B_2O_3(l,s) + 6H_2(g). \quad (6)$$

3.2.2 EDS, XRD, and XPS analyses

To further verify the occurrence of the weight gain reactions, EDS and XRD analyses are employed. As shown in Figure 5a, only the C and O elements are detected on the surface of carbon microspheres without TiB_2 and B_4C. As shown in Figure 5c, the molar ratio of oxygen and titanium in white spot is approximately equal to 5.38, while the molar ratio of TiO_2 is 2. These results implied that new substance was formed and coated on the surface of carbon microspheres. Figure 5d shows the XRD patterns of the residues for TB/C-30 aerogel composites at 25–1,200°C. There are TiB_2 and B_4C diffraction peaks in the non-carbonized aerogel samples. The diffraction peak of TiO_2 can be evidently detected at 800°C, which confirms the oxidation of TiB_2. Besides, broad peak *e* observed at 2θ angles of about 25° is the characteristic peak of amorphous carbon.

The oxygen, titanium, nitrogen, carbon, and boron elements are detected from the full-scan XPS spectrum of the thermal residues (Figure 6a). The high-resolution B1s XPS spectrum for the thermal residues (Figure 6b) shows a prominent peak at 193.28 eV, usually assigned to the contribution of B_2O_3, and the peak detected at energy (190.38 eV) corresponds to the B–O binding [34]. The diffraction peaks of B_2O_3 are not detected by XRD due to its amorphous form in the aerogel network, which has flowability at high temperature (melting point is 450°C) [35–37]. The glassy B_2O_3 could cover the surface of the carbon aerogel by forming a continuous protective film and improving the oxidation resistance of composites.

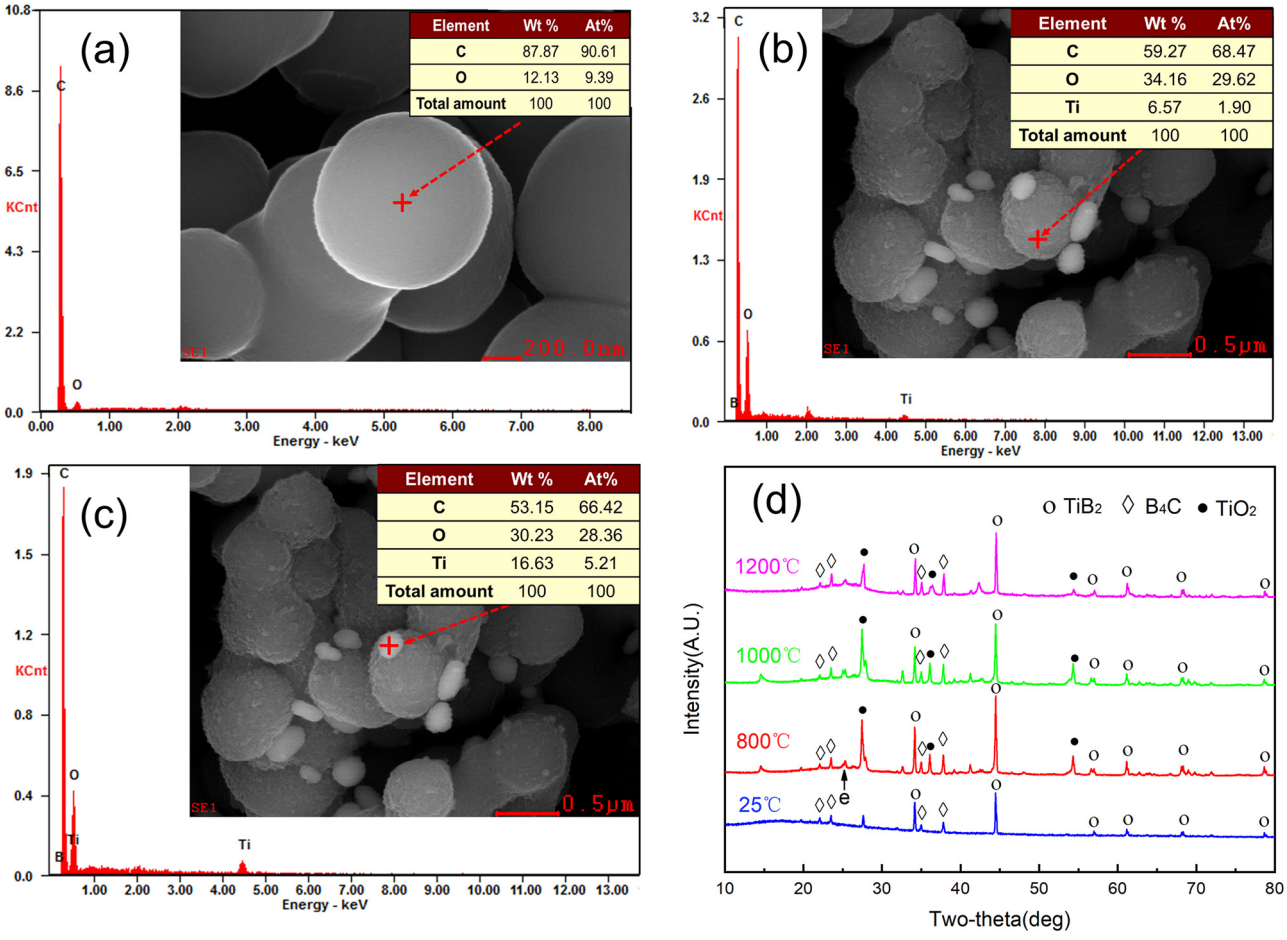

Figure 5: EDS analysis of aerogel composites: (a) TB/C-0; (b and c) TB/C-30; (d) XRD pattern of the TB/C-30 aerogel composites. wt%: mass fraction, At%: atomic fraction.

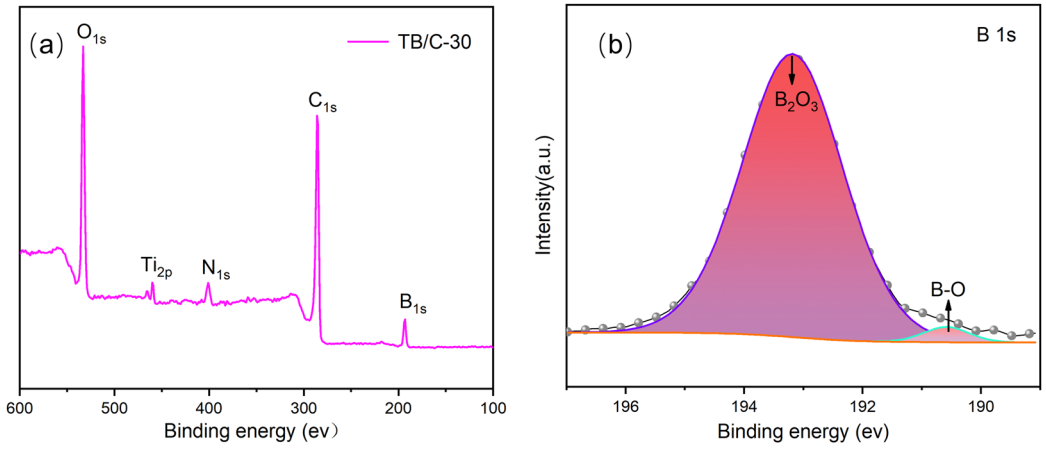

Figure 6: XPS spectra of TB/C-30 aerogel composites: (a) a full-scan and (b) B1s.

3.2.3 Microstructure of TB/C aerogel composites at different carbonization temperatures

Figure 7 illustrates the microstructure transformation of TB/C aerogel composites at different carbonization temperatures. As shown in Figure 7a2, the TB/C-30-800 exhibits typical aerogel network with overlapping structure, and the TiO_2 grains are randomly dispersive and coated on the surface of aerogel nanospheres. The presence of B_2O_3 can densify the surface of aerogel nanospheres and form a protective barrier against high-temperature oxidation. As the carbonization temperature reaches to 1,200°C, the aerogel composites maintain a stable porous nanostructure and form bigger TiO_2 grains with the size of 100 nm (Figure 7c2).

3.3 Mechanical and thermal insulation properties

As shown in Figure 8a, densities of TB/Ph aerogel composites increase remarkably from 0.379 to 0.582 g cm^{-3} with the increased content of TiB_2 and B_4C. This should

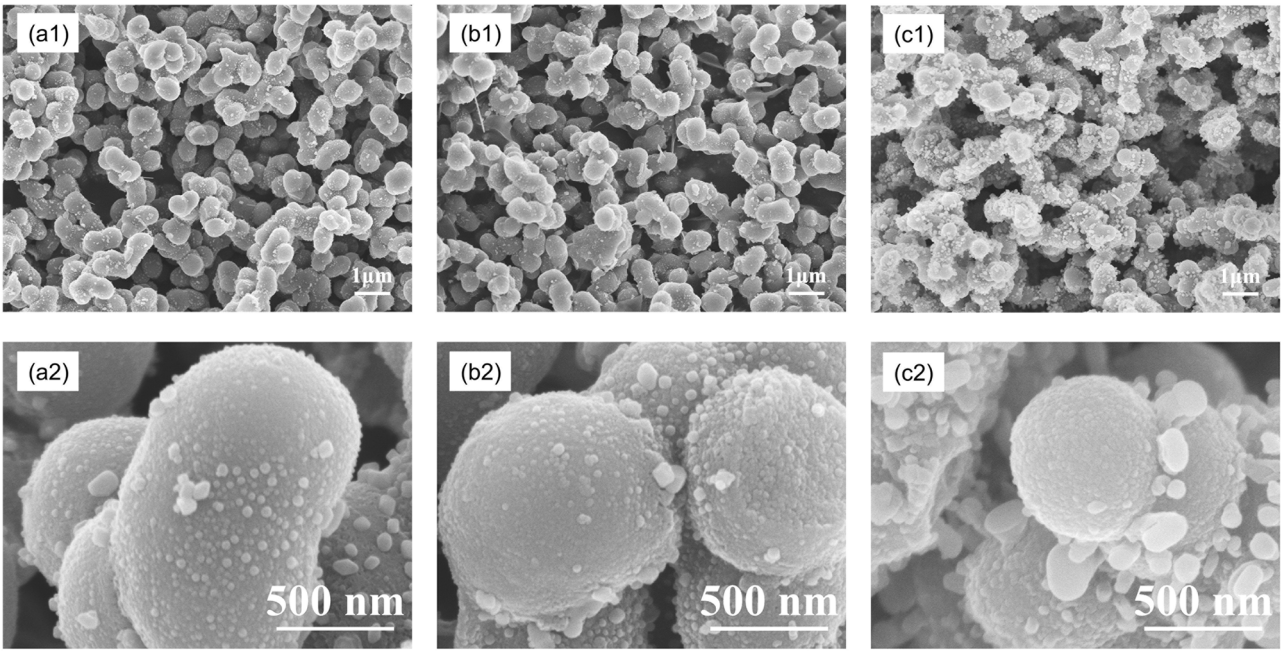

Figure 7: (a)–(c) SEM images of TB/C-30 aerogel composites at different carbonization temperatures: (a1), (a2) 800°C; (b1), (b2) 1,000°C; and (c1), (c2) 1,200°C.

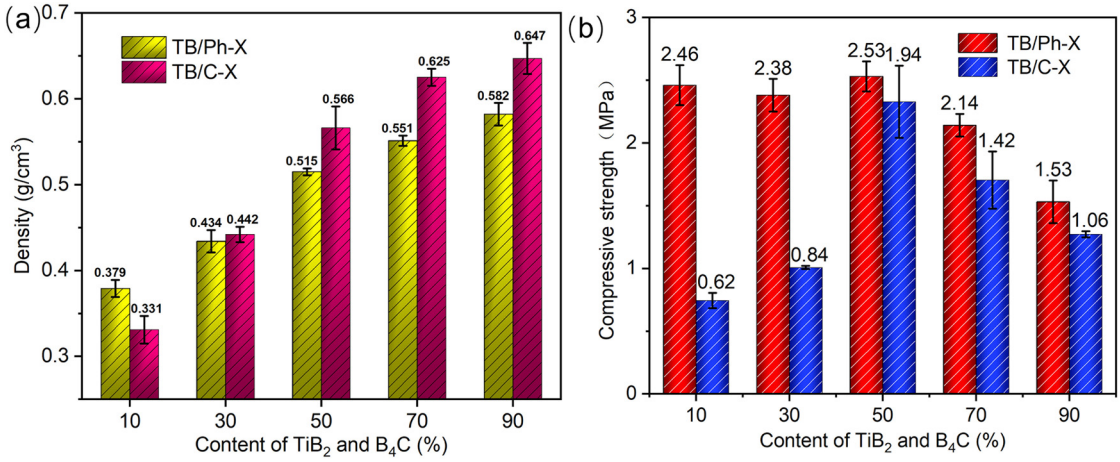

Figure 8: (a) Density of samples and (b) comprehensive strength of samples.

be attributed to the introduction of TiB_2 (4.52 g cm^{-3}) and B_4C (2.52 g cm^{-3}) particles [38]. The density of the TB/C-90 aerogel composites increases slightly from 0.582 to 0.647 g cm^{-3}, majorly due to some weight gain reactions during the carbonization process. Figure 8b presents the compressive strength of samples. The lowest compressive strength of TB/Ph aerogel composites is shown by TB/Ph-90, which also should be attributed to the introduction of TiB_2 and B_4C in aerogels. The increase of TiB_2 and B_4C particles will affect the sol–gel polymerization of organic clusters and eventually weaken the network skeleton of TB/Ph aerogel composites [39–41], which is consistent with the FTIR spectra. Interestingly, it is apparent that the compressive strength of the TB/C aerogel composites first increased from 0.62 to 1.94 MPa and then decreased from 1.94 to 1.06 MPa with a further increase in TiB_2 and B_4C contents (Figure 8b). This should be attributed to the formation of protective structure, which can reduce the pyrolysis of phenolic aerogel matrix and retain its strength. However, TiO_2 grains and glassy B_2O_3 are not assembled into a solid unified structure due to the short carbonization time (only 20 min). Therefore, with the increase of TiB_2 and B_4C contents, the compressive strength will still show a downward trend, which is similar to the compressive performance trend of uncarbonized aerogels.

As displayed in Figure 9a, the drying shrinkage dropped remarkably from 6.03 to 1.85% with the rise of TiB_2 and B_4C contents. This phenomenon can be explained by particle enhancement. With the increase of TiB_2 and B_4C contents, TB/Ph aerogel composites can more effectively against shrinkage due to the huge capillary force generated during ambient pressure drying. Figure 9b illustrates the change of carbonization shrinkage

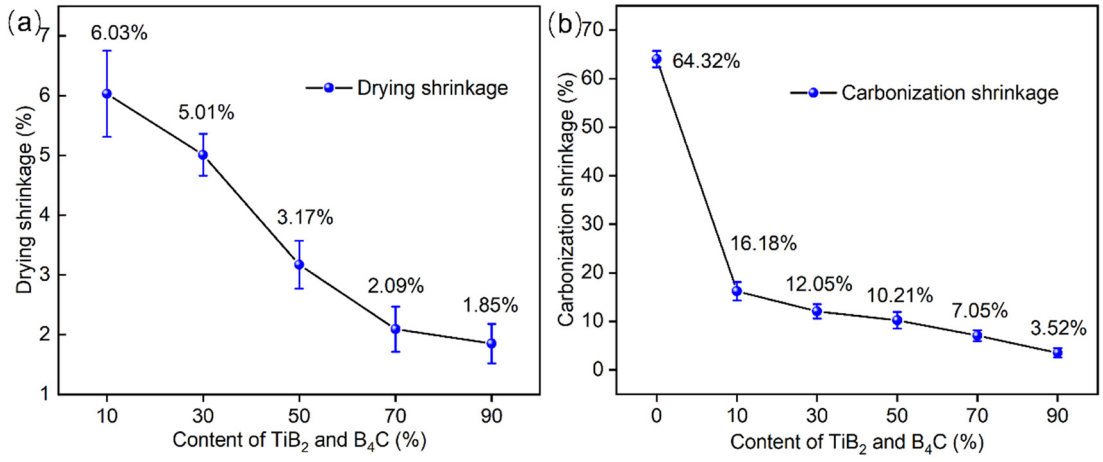

Figure 9: (a) Drying shrinkage of samples and (b) carbonization shrinkage of samples.

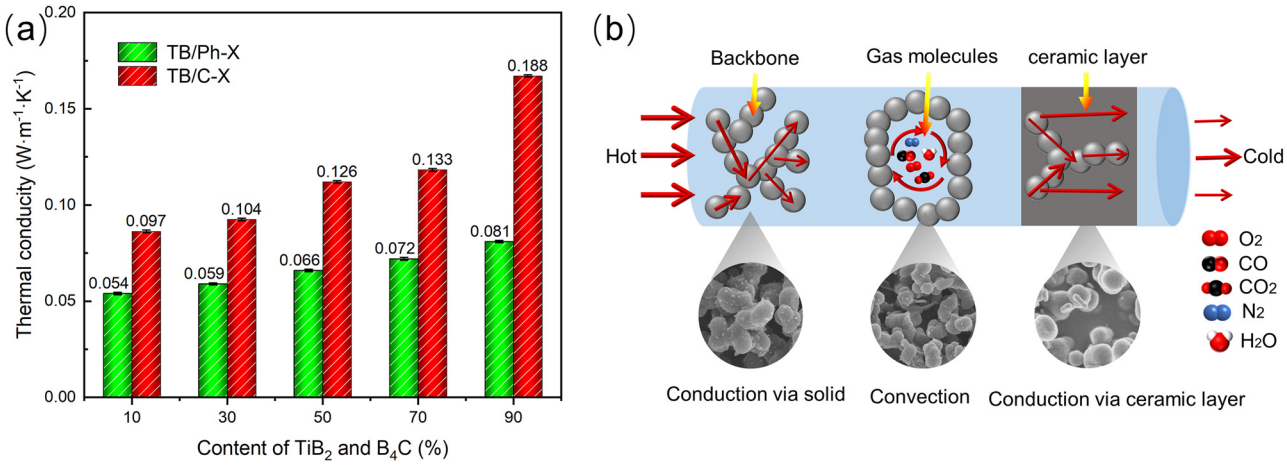

Figure 10: (a) Thermal conductivity curves at 25°C of aerogel composites; (b) schematics illustrating thermal transport pathways.

from TB/Ph to TB/C aerogel composites during carbonization process. The carbonization shrinkage decreases dramatically from 16.18 to 3.52% when changing the content of TiB_2 and B_4C from 10 to 90%, revealing that the introduction of TiB_2 and B_4C particles can effectively restrain the oxidation and improve mechanical properties of composites due to the formation of TiO_2–B_2O_3 layer.

The thermal conductivities of TB/Ph and TB/C aerogel composites were measured at 25°C, and the results are shown in Figure 10a. Typically, the total thermal conductivity includes solid conductivity, gas conductivity, convection transmission, and radiation transmission [42], which can be schematically illustrated in Figure 10b. As the content of TiB_2 and B_4C particles increases, the thermal conductivities of TB/C aerogel composites gradually increase from 0.054 to 0.081 $W\,m^{-1}\,K^{-1}$ at 25°C. On the one hand, the solid phase thermal conductivity increases ascribed to the high thermal conductivity of TiB_2 and B_4C (about 60–120 $W\,m^{-1}\,K^{-1}$) [43]. On the other hand, the aggregation of particles is beneficial to solid-phase thermal conductivity, which will provide more solid-phase thermal transport pathways with the increase in density of the composites. When the content of TiB_2 and B_4C is 90%, the thermal conductivity of TB/Ph-90 aerogel composites is 0.081 $W\,m^{-1}\,K^{-1}$, which increased by 70% compared with those of pure phenolic aerogels (0.048 $W\,m^{-1}\,K^{-1}$).

During carbonization process, the TiB_2 and B_4C particles gradually transform to TiO_2 grains and glassy B_2O_3 by oxidation reaction, which will fill the gap of aerogel microspheres and further improve the solid-phase thermal conductivity of TB/C aerogel composites. When the content of TiB_2 and B_4C is 90%, the thermal conductivity of TB/C-90 aerogel composites is 0.188 $W\,m^{-1}\,K^{-1}$, which increased by 132.11% compared with TB/C-90 aerogel composites (0.081 $W\,m^{-1}\,K^{-1}$). However, due to the porous structures, the heat transfers of gaseous thermal conduction and convection in TB/C aerogel composites are inhibited effectively.

4 Conclusion

By adjusting the content of TiB_2 and B_4C particles, a novel TB/C aerogel composite was fabricated *via* the sol–gel polymerization followed by ambient pressure drying and carbonization. During carbonization process, the TiB_2 and B_4C particles gradually transform to TiO_2 grains and glassy B_2O_3 layer by oxidation reduction reaction, which densify the surface of aerogel nanospheres and form a protective barrier. The resulting TB/C aerogel composites exhibited low densities between 0.331 and 0.647 $g\,cm^{-3}$, relatively high compressive strength, ranging from 0.62 to 1.94 MPa, and low thermal conductivities of 0.097–0.188 $W\,m^{-1}\,K^{-1}$ at room temperature. When the content of TiB_2 and B_4C was 90%, the residue yield of aerogel composites was 90.01% at 1,000°C in air, which increased by 84.33% compared with that of phenolic aerogels. Therefore, this work provides a significant way to improve the oxidation resistance and mechanical properties of TB/Ph aerogel composites, and it may be useful for thermal structure in TPS, such as hypersonic vehicles and civil industrial architectures.

Funding information: This research was financially supported by the Joint Fund of Ministry of Education for Equipment Pre-research (6141A02022250).

Author contributions: All authors have accepted responsibility for the entire content of this manuscript and approved its submission.

Conflict of interest: The authors state no conflict of interest.

References

[1] He H, Geng L, Liu F, Ma B, Huang W, Qu L, et al. Facile preparation of a phenolic aerogel with excellent flexibility for thermal insulation. Eur Polym J. 2022;163:110905.

[2] Jia X, Dai B, Zhu Z, Wang J, Qiao W, Long D, et al. Strong and machinable carbon aerogel monoliths with low thermal conductivity prepared *via* ambient pressure drying. Carbon. 2016;108:551–60.

[3] Balaji A, Udhayasankar R, Karthikeyan B, Swaminathan J, Purushothaman R. Mechanical and thermal characterization of bagasse fiber/coconut shell particle hybrid biocomposites reinforced with cardanol resin. Results Chem. 2020;2:100056.

[4] Yang Z, Li J, Xu X, Pang S, Hu C, Guo P, et al. Synthesis of monolithic carbon aerogels with high mechanical strength *via* ambient pressure drying without solvent exchange. J Mater Sci & Technol. 2020;50:66–74.

[5] Wang Y, Wang S, Bian C, Zhong Y, Jing X. Effect of chemical structure and cross-link density on the heat resistance of phenolic resin. Polym Degrad Stab. 2015;111:239–46.

[6] Wang C, Cheng H, Hong C, Zhang X, Zeng T. Lightweight chopped carbon fibre reinforced silica-phenolic resin aerogel nanocomposite: Facile preparation, properties and application to thermal protection. Compos Part A Appl Sci Manuf. 2018;112:81–90.

[7] Kango S, Kalia S, Celli A, Njuguna J, Habibi Y, Kumar R. Surface modification of inorganic nanoparticles for development of organic–inorganic nanocomposites–A review. Prog Polym Sci. 2013;38(8):1232–61.

[8] Prabhu P, Karthikeyan B, Vannan RR, Balaji A. Dynamic mechanical analysis of Silk and Glass (S/G/S)/Pineapple and Glass (P/G/P)/Flax and Glass (F/G/F) reinforced Lannea coromandelica blender hybrid nano composites. J Mater Res Technol. 2021;15:2484–96.

[9] Pulci G, Paglia L, Genova V, Bartuli C, Valente T, Marra F. Low density ablative materials modified by nanoparticles addition: Manufacturing and characterization. Compos Part A: Appl Sci Manuf. 2018;109:330–7.

[10] Liu H, Wang P, Zhang B, Li H, Li J, Li Y, et al. Enhanced thermal shrinkage behavior of phenolic-derived carbon aerogel-reinforced by HNTs with superior compressive strength performance. Ceram Int. 2021;47(5):6487–95.

[11] Ding J, Huang Z, Qin Y, Shi M, Huang C, Mao J. Improved ablation resistance of carbon–phenolic composites by introducing zirconium silicide particles. Compos Part B: Eng. 2015;82:100–7.

[12] Wang S, Huang H, Tian Y, Huang J. Effects of SiC content on mechanical, thermal and ablative properties of carbon/phenolic composites. Ceram Int. 2020;46(10, Part B):16151–6.

[13] Wu K, Zhou Q, Cao J, Qian Z, Niu B, Long D. Ultrahigh-strength carbon aerogels for high temperature thermal insulation. J Colloid Interface Sci. 2022;609:667–75.

[14] Hou X, Zhang R, Fang D. An ultralight silica-modified ZrO_2–SiO_2 aerogel composite with ultra-low thermal conductivity and enhanced mechanical strength. Scr Materialia. 2018;143:113–6.

[15] Cao X, Wang B, Ma X, Feng L, Shen X, Wang C. Oxidation behavior of melt-infiltrated SiC–TiB_2 ceramic composites at 500–1300°C in air. Ceram Int. 2021;47(7, Part A):9881–7.

[16] Chen Y, Chen P, Hong C, Zhang B, Hui D. Improved ablation resistance of carbon–phenolic composites by introducing zirconium diboride particles. Compos Part B: Eng. 2013;47:320–5.

[17] Amirsardari Z, Mehdinavaz Aghdam R, Salavati-Niasari M, Shakhesi S. Enhanced thermal resistance of GO/C/phenolic nanocomposite by introducing ZrB_2 nanoparticles. Compos Part B: Eng. 2015;76:174–9.

[18] Mulik S, Sotiriou-Leventis C, Leventis N. Time-efficient acid-catalyzed synthesis of resorcinol–formaldehyde aerogels. Chem Mater. 2007;19(25):6138–44.

[19] Zhang Z, Zhao S, Chen G, Feng J, Feng J, Yang Z. Influence of acid-base catalysis on the textural and thermal properties of carbon aerogel monoliths. Microporous Mesoporous Mater. 2020;296:109997.

[20] Singh KP, Palmese GR. Enhancement of phenolic polymer properties by use of ethylene glycol as diluent. J Appl Polym Sci. 2004;91(5):3096–106.

[21] Paulraj P, Balakrishnan K, Rajendran RRMV, Alagappan B. Investigation on recent research of mechanical properties of natural fiber reinforced polymer (NFRP) materials. Materiale Plastice. 2021;58(2):100–18.

[22] Hashimoto M, Tajima F, Yamamura K. Tetrameric O–H···O hydrogen-bond systems accompanied by C–H···O hydrogen-bonds in the crystal of 1,4-bis(hydroxymethyl)triptycene: An X-ray study. J Mol Structure. 2002;616(1):129–34.

[23] Böger T, Sanchez-Ferrer A, Richter K. Hydroxymethylated resorcinol (HMR) primer to improve the performance of wood-adhesive bonds – A review. Int J Adhes Adhesives. 2022;113:103070.

[24] Monk JD, Bucholz EW, Boghozian T, Deshpande S, Schieber J, Bauschlicher CW, et al. Computational and experimental study of phenolic resins: Thermal–mechanical properties and the role of hydrogen bonding. Macromolecules. 2015;48(20):7670–80.

[25] Guo M, Pitet LM, Wyss HM, Vos M, Dankers PYW, Meijer EW. Tough stimuli-responsive supramolecular hydrogels with hydrogen-bonding network junctions. J Am Chem Soc. 2014;136(19):6969–77.

[26] Yi Z, Zhang J, Zhang S, Gao Q, Li J, Zhang W. Synthesis and mechanism of metal-mediated polymerization of phenolic resins. Polymers. 2016;8(5):159.

[27] Giannetti E. Thermal stability and bond dissociation energy of fluorinated polymers: A critical evaluation. J Fluor Chem. 2005;126(4):623–30.

[28] Furer VL, Vandyukov AE, Khamatgalimov AR, Kleshnina SR, Solovieva SE, Antipin IS, et al. Investigation of hydrogen bonding in p-sulfonatocalix[4]arene and its thermal stability by vibrational spectroscopy. J Mol Structure. 2019;1195:403–10.

[29] An X, Jing B, Li Q. Regulating function of alkali metal on the strength of OH···O hydrogen bond in phenol–water complex: Weak to strong and strong to weak. Comput Theor Chem. 2011;966(1):278–83.
[30] Kılıçarslan A, Toptan F, Kerti I, Piskin S. Oxidation of boron carbide particles at low temperatures. Mater Lett. 2014;128:224–6.
[31] Asaro L, D'Amico DA, Alvarez VA, Rodriguez ES, Manfredi LB. Impact of different nanoparticles on the thermal degradation kinetics of phenolic resin nanocomposites. J Therm Anal Calorim. 2017;128(3):1463–78.
[32] Wang J, Jiang H, Jiang N. Study on the pyrolysis of phenol-formaldehyde (PF) resin and modified PF resin. Thermochim Acta. 2009;496(1):136–42.
[33] Deng Z, Yue J, Huang Z. Solvothermal degradation and reuse of carbon fiber reinforced boron phenolic resin composites. Compos Part B: Eng. 2021;221:109011.
[34] Wang S, Wang Y, Bian C, Zhong Y, Jing X. The thermal stability and pyrolysis mechanism of boron-containing phenolic resins: The effect of phenyl borates on the char formation. Appl Surf Sci. 2015;331:519–29.
[35] Li B, Deng J, Li Y. Oxidation behavior and mechanical properties degradation of hot-pressed $Al_2O_3/ZrB_2/ZrO_2$ ceramic composites. Int J Refractory Met Hard Mater. 2009;27(4):747–53.
[36] Brach M, Sciti D, Balbo A, Bellosi A. Short-term oxidation of a ternary composite in the system AlN–SiC–ZrB_2. J Eur Ceram Soc. 2005;25(10):1771–80.
[37] Guo W-M, Zhang G-J, Kan Y-M, Wang P-L. Oxidation of ZrB_2 powder in the temperature range of 650–800°C. J Alloy Compd. 2009;471(1):502–6.
[38] Song Q, Zhang Z-H. Microstructure and self-healing mechanism of B_4C– TiB_2– SiC composite ceramic after pre-oxidation behaviour. Ceram Int. 2022;48(17):25458–64.
[39] Fu S-Y, Feng X-Q, Lauke B, Mai Y-W. Effects of particle size, particle/matrix interface adhesion and particle loading on mechanical properties of particulate–polymer composites. Compos Part B: Eng. 2008;39(6):933–61.
[40] Feng J, Venna SR, Hopkinson DP. Interactions at the interface of polymer matrix-filler particle composites. Polymer. 2016;103:189–95.
[41] Pérez E, Alvarez V, Pérez CJ, Bernal C. A comparative study of the effect of different rigid fillers on the fracture and failure behavior of polypropylene based composites. Compos Part B: Eng. 2013;52:72–83.
[42] Wang G, Zhao J, Wang G, Mark LH, Park CB, Zhao G. Low-density and structure-tunable microcellular PMMA foams with improved thermal-insulation and compressive mechanical properties. Eur Polym J. 2017;95:382–93.
[43] Vajdi M, Sadegh Moghanlou F, Nekahi S, Ahmadi Z, Motallebzadeh A, Jafarzadeh H, et al. Role of graphene nano-platelets on thermal conductivity and microstructure of TiB_2–SiC ceramics. Ceram Int. 2020;46(13):21775–83.